Multinuclear Magnetic Resonance Spectroscopy of Centered Zirconium Halide Clusters

**Jerry D. Harris and Timothy Hughbanks***

Contribution from the Department of Chemistry, Texas A&M University, College Station, Texas 77843-3255

Received April 30, 1997. Revised Manuscript Received July 25, 1997[⊗]

Abstract: Nuclear magnetic resonance spectra for each of the interstitials within centered $[(Zr_6Z)Cl^i{}_{12}Cl^a{}_{6-n}L_n]^{m-}$ clusters (Z = Be, B, C, N, Mn, and Co; L = Cl^-, $AlCl_4{}^-$, CH_3CN, and/or PPh_3; $n = 0-6$) are reported. For C- and Mn-centered clusters, chemical shifts for both solids and solutions have been measured. Chemical shifts for B-centered clusters were measured in solution. Chemical shifts for Be-, N-, and Co-centered clusters were measured in the solid state. Interstitial carbide resonances for all 10 axially substituted species ($\{[(Zr_6C)Cl_{12}](CH_3CN)_nCl_{6-n}\}^{n-4}$, $n = 0-6$) have been located; their chemical shifts range from 457.7 ppm for $\{[(Zr_6C)Cl_{12}]Cl_6\}^{4-}$ to 480.1 ppm for $\{[(Zr_6C)Cl_{12}](CH_3CN)_6\}^{2+}$. ^{11}B chemical shifts for boride-centered clusters ($\{[(Zr_6B)Cl_{12}](CH_3CN)_nCl_{6-n}\}^{n-5}$, $n = 0-5$) range from 185 to 193.8 ppm. ^{11}B and ^{13}C data reveal the axially bound chlorides to be substitutionally inert. Chemical shifts for ^{55}Mn-centered clusters range from 5359 ppm (isotropic) for solid $RbZr_6Cl_{14}Mn$ to 5618 ppm for $[(Zr_6Mn)Cl_{12}Cl_6]^{5-}$ in a Cl^--rich molten salt. These are the most deshielded manganese compounds presently known. Solid-state ^9Be for $K_3Zr_6Cl_{15}Be$, ^{15}N for $Zr_6Cl_{15}N$, and ^{59}Co for $Zr_6Cl_{15}Co$ reveal chemical shifts of 77.1, 271, and 4082 ppm, respectively (the ^9Be data is not corrected for the second-order quadrupolar contribution). A discussion of the origin of large paramagnetic shielding contributions to the chemical shifts of the interstitial atoms is given.

Introduction

Exploration of the solution chemistry of centered zirconium halide clusters $[(Zr_6Z)Cl^i{}_{12}L^a{}_6]^{m-}$ (**1**), (Z = H, Be, B, C, N, Mn, Fe, and Co) has been ongoing for the past few years.[1−10]
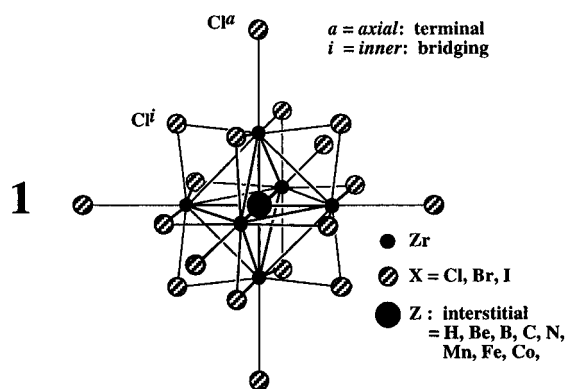
An obstacle to the efficient development of this chemistry has been the nearly exclusive reliance on crystallography as a means of characterization; where crystalline products have been elusive,

characterization has been scant. Although each of the different centered cluster possesses a unique electronic spectrum, such a spectrum serves mainly to indicate whether the cluster core remains intact in solution. Since features in the near-IR, visible, and near-UV electronic spectra arise from transitions within the metal-based orbital manifold,[4] one obtains little information as to the axial ligands change, and therefore little information emerges as to the number and kind of ligands bound to each cluster. On the other hand, the presence of interstitial atoms in these clusters offers the prospect of using multinuclear NMR to monitor the clusters' chemistry. Because of the locally octahedral environment of the interstitial atom, even for nuclei with sizable quadrupole moments, reasonably narrow line widths should be obtained.

Although Corbett and co-workers measured ^1H and ^{13}C NMR chemical shifts in a few of the solid-state cluster precursors,[11−15] such information has not been systematized, and it has not been exploited for analytical purposes. We have therefore set out to establish benchmark measurements to enable future routine use of NMR spectroscopy as an analytical tool in studying this chemistry. Of course, these measurements also provide interesting information about the electronic environment within hexanuclear zirconium clusters.

Of the known $[(Zr_6Z)Cl^i{}_{12}L^a{}_6]^{m-}$ clusters, nearly all of the interstitials (Z) have NMR-active isotopes. To date, all known H-centered zirconium clusters from solid-state synthesis are paramagnetic and are not easily amenable to NMR study. ^{57}Fe has a 2.19% natural abundance and a relative sensitivity of 3.4

* Author to whom correspondence should be addressed.
⊗ Abstract published in *Advance ACS Abstracts,* September 15, 1997.
(1) Rogel, F.; Corbett, J. D. *J. Am. Chem. Soc.* **1990**, *112*, 8198−8200.
(2) Rogel, F.; Zhang, J.; Payne, M. W.; Corbett, J. D. In *Electron Transfer in Biology and the Solid State*; Johnson, M. K., King, R. B., Kurtz, D. M., Jr., Kutal, C., Norton, M. L., Scott, R. A., Ed.; American Chemical Society: Washington, DC, 1990; Vol. 226, pp 367−389.
(3) Rogel, F. Ph.D. Thesis, Iowa State University, 1990.
(4) Bond, M. R.; Hughbanks, T. *Inorg. Chem.* **1992**, *31*, 5015−5021.
(5) Runyan, C. E., Jr.; Hughbanks, T. *J. Am. Chem. Soc.* **1994**, *116*, 7909−7910.
(6) Runyan, C. E., Jr. Ph.D. Thesis, Texas A&M University, 1994.
(7) Tian, Y.; Hughbanks, T. *Inorg. Chem.* **1995**, *34*, 6250−6254.
(8) Tian, Y.; Hughbanks, T. *Z. Anorg. Allg. Chem.* **1996**, *622*, 425−431.
(9) Harris, J. D.; Hughbanks, T. *J. Cluster Sci.* **1997**, in press.
(10) Runyan, C. E., Jr.; Harris, J. D.; Hughbanks, T. To be submitted.

(11) Fry, C. G.; Smith, J. D.; Gerstein, B. C.; Corbett, J. D. *Inorg. Chem.* **1986**, *25*, 117−118.
(12) Chu, P. J.; Ziebarth, R. P.; Corbett, J. D.; Gerstein, B. C. *J. Am. Chem. Soc.* **1988**, *110*, 5324−5329.
(13) Zhang, J.; Corbett, J. D. *Inorg. Chem.* **1991**, *30*, 431−435.
(14) Zhang, J.; Ziebarth, R. P.; Corbett, J. D. *Inorg. Chem.* **1992**, *31*, 614−619.
(15) Zhang, J.; Corbett, J. D. *J. Solid State Chem.* **1994**, *109*, 265−271.

$\times$ 10^{-5} (compared to ^{1}H, this is $\sim^1/_{480}$ that of ^{13}C),[16] so it too was not investigated. All the remaining isotopes (Z = ^{9}Be, ^{11}B, ^{13}C, ^{15}N, ^{55}Mn, and ^{59}Co), exhibit reasonable sensitivity and have either high natural abundance or can be readily obtained in an isotopically enriched form.

In this paper we present solid-state or both solid- and solution-state NMR data for Be-, B-, C-, N-, Mn-, and Co-centered clusters. Solution NMR spectra were obtained in both acetonitrile and a room-temperature molten salt composed of 1-ethyl-3-methylimidazolium chloride (ImCl) and aluminum trichloride. The latter can be prepared with ImCl/AlCl$_3$ ratios that yield melts that are Lewis basic, neutral, or Lewis acidic. A substantial amount of electrochemical work on clusters has been done using these ionic liquids,[17-20] but only recently have these melts been used for excision of clusters from solid precursors.[5,7,8]

Experimental Section

Techniques and Materials. Manipulation of all compounds was performed either in an inert atmosphere (N$_2$) glovebox or on a Schlenk (Ar) or high-vacuum line. All glassware and syringe needles were oven dried (160 °C) overnight before use. Absorption spectra were recorded using a Cary 219 UV–visible spectrometer at room temperature. A set of matched cuvettes (2 mm path length) was used for each measurement to correct for the absorbance of the solvent.

Cluster-containing materials were synthesized as reported elsewhere.[13,14,21-24] They were generally prepared by heating stoichiometric quantities of alkali metal chloride, ZrCl$_4$, Zr powder and Be (Aldrich), B (Alfa) or ^{13}C (Isotec Inc., 99.1% ^{13}C) powders, ^{15}NH$_4$Cl (Aldrich, 98% ^{15}N), MnCl$_2$ or FeCl$_3$ in Nb tubes, which were sealed under vacuum in fused silica jackets and heated at 850 °C for 2–4 weeks. All compounds were identified by Guinier X-ray powder diffraction. Alkali-metal chlorides, ZrCl$_4$, MnCl$_2$, FeCl$_3$ and CoCl$_2$ were sublimed under vacuum prior to use. Zr powder was prepared from Zr foil by a hydrogenation–dehydrogenation reaction that has been described previously.[25] Be, B, and ^{13}C powders and ^{15}NH$_4$Cl were used as received.

All deuterated solvents were used as received and stored under N$_2$. Nondeuterated acetonitrile (spectroscopic grade, Aldrich) was dried by refluxing over CaH$_2$ overnight and then distilling under N$_2$ before use. Triphenylphosphine (PPh$_3$) was sublimed prior to use. Bis(triphenylphosphoranylidene)ammonium chloride (PPNCl) was dried by an azeotropic distillation in CH$_3$CN.

1-Ethyl-3-methylimidazolium chloride (ImCl) was prepared by reacting ethyl chloride with freshly distilled methylimidazole following a procedure described by Wilkes and co-workers.[26-28] The salt was

(16) Weast, R. C.; Astle, M. J.; Beyer, W. H. *Handbook of Chemistry and Physics*, 67th ed.; Weast, R. C., Astle, M. J., Beyer, W. H., Eds.; CRC Press, Inc: Boca Raton, FL, 1986.
(17) Hussey, C. L. In *Chemistry of Nonaqueous Solutions*; Mamantov, G., Popov, A. I., Eds.; VCH: New York, 1994; pp 227–276.
(18) Barnard, P. A.; Sun, I.-W.; Hussey, C. L. *Inorg. Chem.* **1990**, *29*, 3670–3674.
(19) Quigley, R.; Barnard, P. A.; Hussey, C. L.; Seddon, K. R. *Inorg. Chem.* **1992**, *31*, 1255–1261.
(20) Hussey, C.; Quigley, R.; Seddon, K. *Inorg. Chem.* **1995**, *34*, 370–377.
(21) Ziebarth, R. P.; Corbett, J. D. *J. Am. Chem. Soc.* **1988**, *110*, 1132–1139.
(22) Ziebarth, R. P.; Corbett, J. D. *J. Am. Chem. Soc.* **1989**, *111*, 3272–3280.
(23) Ziebarth, R. P.; Corbett, J. D. *J. Am. Chem. Soc.* **1987**, *109*, 4844–4850.
(24) Ziebarth, R. P.; Corbett, J. D. *J. Less-Common Met.* **1988**, *137*, 21–34.
(25) Smith, J. D.; Corbett, J. D. *J. Am. Chem. Soc.* **1985**, *107*, 5704–5711.
(26) Strubinger, S. K. D.; Sun, I. W.; Cleland, W. E., Jr.; Hussey, C. L. *Inorg. Chem.* **1990**, *29*, 4246–4252.
(27) Strubinger, S. K. D.; Sun, I.-W.; Cleland, W. E., Jr.; Hussey, C. L. *Inorg. Chem.* **1990**, *29*, 993–999.
(28) Wilkes, J. S.; Levisky, J. A.; Wilson, R. A.; Hussey, C. L. *Inorg. Chem.* **1982**, *21*, 1263–1264.

recrystallized several times from dry acetonitrile and dry ethyl acetate before use. Aluminum trichloride (Aldrich, aluminum chloride anhydrous, 99%) was vacuum sublimed at least three times before use. When ImCl and aluminum trichloride are mixed, they form a room temperature melt that can be prepared over a wide range of compositions (i.e., from Lewis basic where X$_{ImCl}$ > X$_{AlCl_3}$ to Lewis acidic where X$_{ImCl}$ < X$_{AlCl_3}$).

NMR. Solid-state NMR spectra were measured on either a Bruker MSL-300 spectrometer (^{9}Be at 42.17 MHz, ^{13}C at 75.47 MHz, ^{15}N at 30.42 MHz, ^{55}Mn at 74.28 MHz, and ^{59}Co at 71.13 MHz), a Chemagnetics CMX-300 spectrometer (^{55}Mn at 74.28 MHz), or a Chemagnetics CMX-360 spectrometer (^{55}Mn at 89.13 MHz and ^{59}Co at 85.35 MHz). Solution NMR spectra were measured on either a Varian XL 200 broad-band spectrometer (^{11}B at 64.18 MHz, ^{13}C at 50.31 MHz, and ^{55}Mn at 49.56 MHz), or a Varian Unity plus spectrometer, or Varian VXR 300 spectrometer (^{13}C at 75.45 MHz and ^{31}P at 121.43 MHz). Solution spectra were measured in ImCl/AlCl$_3$ melts and CD$_3$CN.

Chemical shifts for ^{9}Be, ^{11}B, ^{31}P, ^{55}Mn, and ^{59}Co were reported with respect to the external standards of Be(H$_2$O)$_4^{2+}$, BF$_3$·OEt$_2$, H$_3$PO$_4$, MnO$_4^-$, and Co(CN)$_6^{3-}$, respectively ($\delta = 0$). Be(H$_2$O)$_4^{2+}$ was prepared as a saturated solution of BeSO$_4$·2H$_2$O in H$_2$O. Chemical shifts for ^{13}C in CH$_3$CN were set using the resonances of CH$_3$CN as an internal standard (1.3 ppm and 118.2 ppm for the methyl and CN respectively relative to SiMe$_4$). Chemical shifts for ^{13}C in ImCl/AlCl$_3$ solutions were set using the resonance from CD$_3$OCD$_3$ as an external standard (29.8 ppm for CD$_3$ relative to SiMe$_4$). The CD$_3$OCD$_3$ was in a coaxial tube to separate it from the ImCl/AlCl$_3$ solution. ^{15}NH$_4$Cl$_{(s)}$, was used as an external reference for ^{15}N solid NMR, set at −341.2 ppm vs neat liquid nitromethane.

1. NMR of KZr$_6$Cl$_{15}$C Dissolved in ImCl/AlCl$_3$ Melts. KZr$_6$-Cl$_{15}$C (61 mg, 0.054 mmol) was loaded into an ampule. ImCl (970 mg, 6.75 mmol) and AlCl$_3$ (441 mg, 3.31 mmol) were mixed in a vial and then the solution ($\sim$0.9 mL) was transferred to the ampule. The ampule was evacuated, sealed, and then put into an oven at 120 °C for 3 days and then in an ultrasonic bath for several more days. The sample was centrifuged and transferred to a 5 mm NMR tube. After the ^{13}C spectrum was measured, the sample was transferred back to a vial and AlCl$_3$ (600 mg, 4.50 mmol) was added to the solution. This Lewis acidic solution was transferred back to the NMR tube.

2. NMR of KZr$_6$Cl$_{15}$C, with Added PPNCl, and with Added PPh$_3$ Dissolved in CH$_3$CN. KZr$_6$Cl$_{15}$C (148 mg, 0.13 mmol), CD$_3$-CN (3.0 mL), CH$_3$CN (1.3 mL), and a stir bar were sealed in an ampule. The solution was stirred for 9 days and centrifuged to remove insoluble solids. One milliliter of this solution was transferred to a 5 mm NMR tube, and the ^{13}C spectrum was measured. The remainder was divided between two additional 5 mm NMR tubes, one containing 104 mg (0.18 mmol) of PPNCl and the second containing 70 mg (0.27 mmol) of PPh$_3$. The ^{13}C spectrum for the tube containing PPNCl was measured 1 day after PPNCl was added; the ^{31}P and ^{13}C spectra for the tube containing PPh$_3$ were measured 3 days after the PPh$_3$ was added.

3. NMR of KZr$_6$Cl$_{15}$C Dissolved in CH$_3$CN with Added TlPF$_6$. KZr$_6$Cl$_{15}$C (131 mg, 0.12 mmol) and CD$_3$CN (3.0 mL) were put into a test tube. The test tube was placed in a ultrasonic bath for 2 days. TlPF$_6$ (249 mg, 0.71 mmol) was dissolved in 0.5 mL of CH$_3$CN and transferred to the test tube. The TlPF$_6$ flask was washed several times with a total volume of 1.4 mL of CH$_3$CN. After centrifugation, the solution was decanted from undissolved starting material and precipitated TlCl, then transferred to a 10 mm NMR tube.

4. NMR of KZr$_6$Cl$_{15}$C with Added NaCl Dissolved in CH$_3$CN. KZr$_6$Cl$_{15}$C (40 mg, 0.035 mmol), NaCl (9 mg, 0.15 mmol), and CD$_3$-CN (1.0 mL) were loaded into a test tube. KZr$_6$Cl$_{15}$C (40 mg, 0.035 mmol) and CD$_3$CN (1.0 mL) were also loaded into a separate tube. Both test tubes were sonicated and then centrifuged. The dark orange solution from both test tubes was transferred to a single 5 mm NMR tube.

5. Variable Temperature NMR of KZr$_6$Cl$_{15}$C with Added NaCl Dissolved in CH$_3$CN. KZr$_6$Cl$_{15}$C (270 mg, 0.24 mmol), NaCl (600 mg, 10.3 mmol), CD$_3$CN (5.0 mL), and a drop or two of CD$_3^{13}$CN were sealed in an ampule. The ampule was heated to 120 °C for 2 days and then placed in an ultrasonic bath overnight. The solution was centrifuged to remove undissolved starting material and then

transferred to a 10 mm NMR tube. The spectrum was measured at −30, 20, 30, 50, and 70 °C.

6. NMR of $Rb_5Zr_6Cl_{18}B$ Dissolved in CH_3CN. $Rb_5Zr_6Cl_{18}B$ (137 mg, 0.084 mmol), CH_3CN (8.0 mL), and a stir bar were added to a test tube. The solution stirred overnight and was then centrifuged to remove undissolved starting material. Four milliliters of solution was transferred to a 10 mm NMR tube containing 0.5 mL of CD_3CN.

7. NMR of $RbZr_6Cl_{14}Mn$ Dissolved in $ImCl/AlCl_3$ Melts. $RbZr_6Cl_{14}Mn$ (130 mg, 0.11 mmol) was loaded into an ampule. ImCl (3.006 g, 20.9 mmol) and $AlCl_3$ (1.435 g, 10.8 mmol) were mixed in a vial, and the solution (∼3.4 mL) was transferred to the ampule. The ampule was evacuated on a high vacuum line overnight, sealed, and put into an oven at 120 °C for 6 days. The sample was then centrifuged, and the solution was transferred to a 10 mm NMR tube. After the spectrum was measured at room temperature, $AlCl_3$ (2.790 g, 20.9 mmol) was added to the solution and the spectrum of the cluster in the acidic melt was measured at both room temperature and 70 °C. ImCl (3.00 g, 20.9 mmol) was added to the solution and the basic solution was measured at 70 °C. A coaxial tube containing D_2O was used to lock and shim the sample.

8. Solid-State NMR Measurements. In most instances, approximately 0.5 g of sample was packed into a solid-state rotor and which was spun at rates ranging from 3.0 to 4.5 kHz as data were acquired. Compounds used were $K_3Zr_6Cl_{15}Be$, $KZr_6Cl_{15}C$, $Zr_6Cl_{15}N$, $RbZr_6Cl_{14}Mn$, $Li_2Zr_6Cl_{15}Mn$, or $Zr_6Cl_{15}Co$. Two additional ^{55}Mn spectra were recorded on $RbZr_6Cl_{14}Mn$ at higher spinning rates (7.5 and 10.0 kHz) at a higher field strength (8.4 T, 89.65 MHz) and two additional ^{59}Co spectra were recorded on $Zr_6Cl_{15}Co$ at higher spinning rates (8.0 and 10.0 kHz) at a higher field strength (8.4 T, 85.70 MHz).

9. Electronic Spectra of $[(Zr_6C)Cl_{12}L_6]^{n-}$ Dissolved in CH_3CN and $ImCl/AlCl_3$ Melts. $KZr_6Cl_{15}C$ (155 mg, 0.137 mmol) and CH_3-CN (10 mL) were loaded into an ampule. The solution was degassed, and then the ampule was sealed. The ampule was put into a 60 °C oven for 6 days and then taken out and put into an ultrasonic bath overnight. The ampule was then centrifuged, and the solution was transferred to a Schlenk flask. The solution was concentrated to 2 mL, and 20 mL of Et_2O was added to precipitate the product. The clear supernatant was removed, and the product was evacuated to dryness; 100 mg of product was recovered and was assumed to be of the composition $K(Zr_6C)Cl_{15}(NCCH_3)_3$. Four milligrams of $K(Zr_6C)Cl_{15}(NCCH_3)_3$ was dissolved in 20 mL of CH_3CN. An aliquot of the solution was transferred to a 2 mm cuvette, and the electronic spectrum was measured with a matched cell containing CH_3CN. Eight milligrams of $K(Zr_6C)Cl_{15}(NCCH_3)_3$, 1.135 g of ImCl, and 2.005 g of $AlCl_3$ were mixed in a vial and made 2.2 mL of solution. One-tenth of a milliliter of this solution was added to 1.150 g (8.01 mmol) ImCl and 2.007 g (15.05 mmol) $AlCl_3$ to yield 2.3 mL of 35:65 $ImCl/AlCl_3$ solution. An aliquot of this solution was transferred to a 2 mm cuvette, and the electronic spectrum was measured with a matched cell containing an $ImCl/AlCl_3$ solution (39:61) prepared by mixing ImCl (0.696 g, 4.85 mmol) and $AlCl_3$ (1.015 g, 7.61 mmol). The cluster solution was then transferred back to the vial and ImCl (1.643 g, 11.44 mmol) was added to make the solution Lewis basic, bringing the total volume of the solution to 3.1 mL. The blank solution was transferred back to a vial, and ImCl (1.634 g, 11.37 mmol) and $AlCl_3$ (0.504 g, 3.78 mmol) were added. Both solutions were transferred back to their respective cuvettes and the electronic spectrum of the cluster solution was measured.

Many of the solutions for NMR measurements were given extensive pretreatment (e.g., long duration stirring, ultrasound treatment, and/or high temperatures) to increase cluster concentrations. Typically, 10000−40000 transients were required to obtain ^{13}C, ^{11}B, and ^{55}Mn data presented here. Because ^{13}C relaxation times are long for both interstitials and CH_3*CN, total acquisition times for this nucleus ranged from 4 to 24 h per spectrum.

Results

When a chloride-supported hexanuclear zirconium cluster dissolves in a coordinating solvent there are, including geometric isomers, 10 distinct species of the type $[(Zr_6Z)Cl_{12}Cl_{6-n}(Solv)_n]^{m-}$ ($n = 0-6$) that can form. If the interstitial in the center of

Table 1. Selected ^{13}C NMR Data for Carbon-Centered Octahedral Clusters

| compound	δ (ppm)	ref
$[(Fe_6C)(CO)_{16}]^{2-}$	484.6	a
$\{[Zr_6Cl_{12}C](NCCH_3)_6\}^{2+}$	480.1	b
$\{[Zr_6Cl_{12}C](AlCl_4)_6\}^{4-}$ in $ImCl/AlCl_3$ (acidic)	471.9	b
$[(Rh_6C)(CO)_{13}]^{2-}$	470	c
$[(Zr_6C)Cl_{18-x}(NCCH_3)_x]^{x-4}$ ($1 \le x \le 5$)	472.9, 470.6, 466.8, 464.9, 463.3, 461.6, 460.2, 459.0	b
$[(Zr_6C)Cl_{17-x}(PPh_3)_x]^{x-3}$ ($0 \le x \le 2$)	464.9, 463.3, 461.6, 460.2, 459.0	b
$KZr_6Cl_{15}C$ (solid)	465.5 (av)	b
$[(Ru_6C)(CO)_{16}]^{2-}$	458.9	a
$\{[Zr_6Cl_{12}C]Cl_6\}^{4-}$ in CH_3CN	457.7	b
$\{[Zr_6Cl_{12}C]Cl_6\}^{4-}$ in $ImCl/AlCl_3$ (basic)	455.5	b
$[(Ru_6C)(CO)_{14}(C_6H_3Me_3)]$	442.8	d
$[(Mo_2Ru_4C)O(CO)_{12}Cp_2]$	438.7	e
$[(Fe_2Ni_3C)(CO)_{13}]^{2-}$	435	f
$[(Re_6C)(CO)_{19}]^{2-}$	421.8	g
$[(Re_6C)H(CO)_{19}]^{-}$	413.5	g
$[(Os_{10}C)(CO)_{24}H]^{-}$ ^{i}	409	h

^{a} Bradley, J. S. *Adv. Organomet. Chem.* **1983**, *22*, 1−58. ^{b} This work. ^{c} Bordoni, S.; Heaton, B. T.; Seregni, C.; Strona, L.; Goodfellow, R. J.; Hursthouse, M. B.; Thornton-Pett, M.; Martinengo, S. *J. Chem. Soc., Dalton Trans.* **1988**, 2103−2108. ^{d} Bailey, P. J.; Duer, M. J.; Johnson, B. F. G.; Lewis, J.; Conole, G.; McPartlin, M.; Powell, H. R.; Anson, C. E. *J. Organomet. Chem.* **1990**, *383*, 441−461. ^{e} Adams, H.; Gill, L. J.; Morris, M. J. *Organometallics* **1996**, *15*, 464−467. ^{f} Hrljac, J. A.; Swepston, P. N.; Shriver, D. F. *Organometallics* **1985**, *4*, 158−166. ^{g} Beringhelli, T.; D'Alfonso, G.; Molinari, H.; Sironi, A. *J. Chem. Soc., Dalton Trans.* **1992**, 689−695. ^{h} Constable, E. C.; Johnson, B. F. G.; Lewis, J.; Pain, G. N.; Taylor, M. J. *J. Chem. Soc., Chem. Commun.* **1982**, 754−756. ^{i} Octahedral core with four faces capped by $Os(CO)_3$ groups yielding T_d symmetry.

each cluster is sensitive to the different environment for each species, each should have a different chemical shift. Also, since the interstitial is isolated inside the Zr_6 cage, each species should be observed as a singlet unless spin−spin couplings are detected.

Carbon-Centered Clusters. The magic-angle spinning (MAS) solid-state NMR for $KZr_6Cl_{15}C$ shows two peaks, one centered at 464.2 ppm and the other centered at 467.1 ppm. This result was expected since there are two crystallographically unique clusters in the $KZr_6Cl_{15}C$ structure.[23] The chemical shift for the carbon is comparable with carbon-centered octahedral metal clusters, despite the fact that most such clusters involve later transition metals with carbonyl ligands (Table 1).

After some preliminary NMR measurements showed that numerous species were present in acetonitrile solutions of C-centered clusters, systematic experiments were carried out to establish the range of ^{13}C chemical shifts to be expected for species with the $[(Zr_6C)Cl_{12}]^{2+}$ core. When $KZr_6Cl_{15}C$ is dissolved in the Lewis basic $ImCl/AlCl_3$ (67:33) melt, a sharp singlet at 455.5 ppm is obtained. Upon titrating the melt into the Lewis acidic regime (46:54) by addition of $AlCl_3$, the only feature observed in the interstitial region of the spectrum is a singlet at 471.9 ppm. When $KZr_6Cl_{15}C$ and excess PPNCl is dissolved in CH_3CN a singlet at 457.7 ppm, (Figure 1, spectrum a, peak J) is observed. When $KZr_6Cl_{15}C$ is dissolved in CH_3-CN and $TlPF_6$ is added to abstract the terminal chlorides, a sharp singlet at 480.1 ppm and a much less intense singlet at 472.9 ppm are obtained (Figure 1, spectrum d, peaks A and B).

As discussed below, the measurements described established the chemical shifts for the two extreme species, $\{[(Zr_6C)Cl_{12}]Cl_6\}^{4-}$ and $\{[(Zr_6C)Cl_{12}](NCCH_3)_6\}^{2+}$. Further measurements were made to locate chemical shifts for the eight intermediate species. When $KZr_6Cl_{15}C$ is dissolved in CH_3CN without any additional ligand, three singlets are observed (Figure
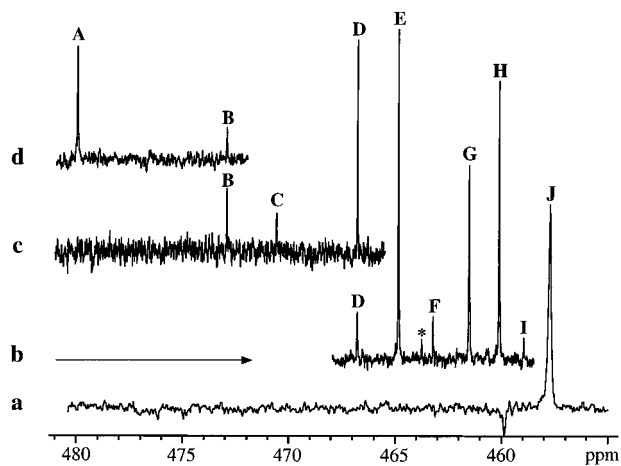
Figure 1. ^{13}C NMR spectra for $KZr_6Cl_{15}C$ dissolved in acetonitrile with (a) added PPNCl, (b) added NaCl, (c) no added ligand, and (d) added $TlPF_6$. Labeled peaks (A−J) correspond to the 10 possible isomers. The singlet labeled with an asterisk is not believed to be from a cluster species.
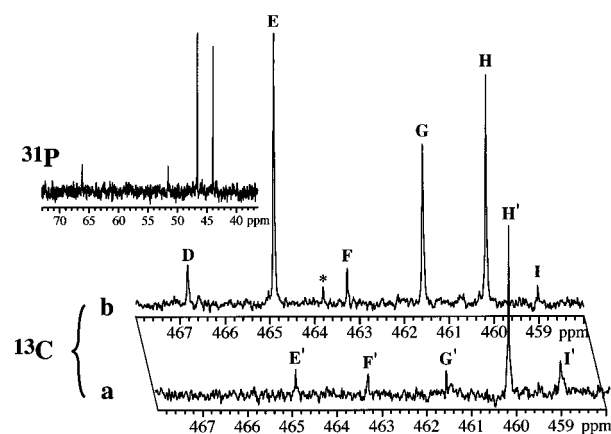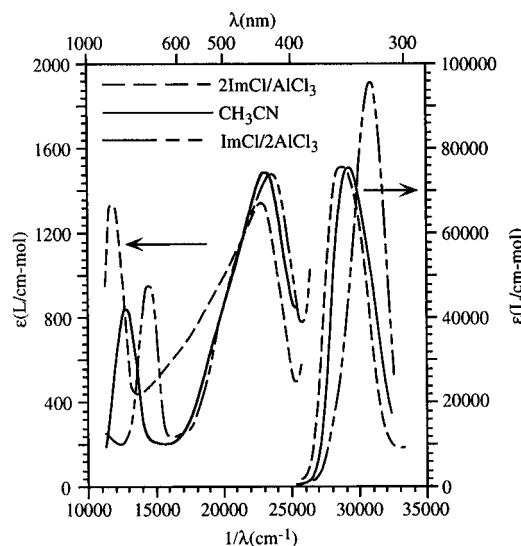

Figure 2. ^{13}C NMR spectra for $KZr_6Cl_{15}C$ dissolved in acetonitrile with (a) added PPh_3, and (b) added NaCl. Labeling of peaks is consistent with Figure 1; phosphine-ligated species are given primed labels. Inset shows ^{31}P NMR spectrum for the sample in a.

1, spectrum c, peaks labeled B−D): an intense singlet at 466.8 ppm and two less intense singlets at 470.6 and 472.9 ppm. On the other hand, if $KZr_6Cl_{15}C$ is dissolved in an acetonitrile solution saturated with NaCl, 5−7 singlets ranging from 459 to 467 ppm are observed (Figure 1, spectrum b, peaks labeled D−I).

When triphenylphosphine was added to a solution prepared by dissolving $KZr_6Cl_{15}C$ in CD_3CN, the ^{13}C NMR shows five singlets (Figure 2): an intense singlet at 460.2 ppm and four weaker singlets at 459.0, 461.6, 463.3, and 464.9 ppm. The ^{31}P NMR was also measured for the solution and revealed four singlets: two intense singlets a 44 and 46.6 ppm and two less intense singlets at 51.5 and 66.2 ppm. No $^2J_{P-Zr-C}$ coupling was observed in either spectrum.

Labeled $CH_3{}^*CN$ was added to a carbide-centered cluster solution to enhance the signal from CH_3CN bound to the cluster. Data for the sample were acquired at −30, 20, 30, 50, and 70 °C. At −30 and 20 °C the spectra were identical, with singlets at 132.8 and 132.1 ppm for the bound acetonitrile. The two singlets from bound acetonitrile disappear at 30 °C and reappear upon cooling back to 20 °C; the region between 455 and 470 ppm remained nearly unchanged over the entire temperature range.

The electronic spectrum of $[(Zr_6C)Cl_{12}L_6]^{m-}$ has been measured in CH_3CN as well as in the $ImCl/AlCl_3$ melts. As the

Figure 3. Electronic spectra for $KZr_6Cl_{15}C$ dissolved in acetonitrile and in basic and acidic $ImCl/AlCl_3$ melts.
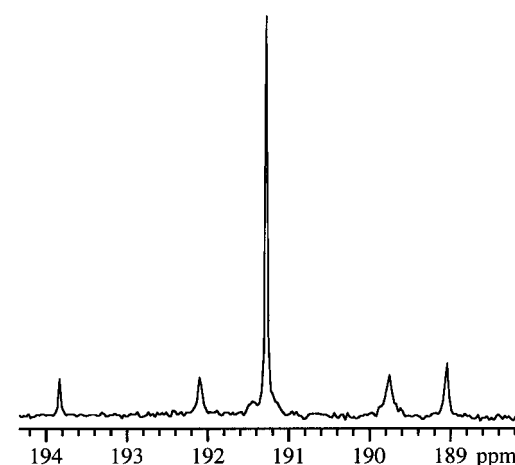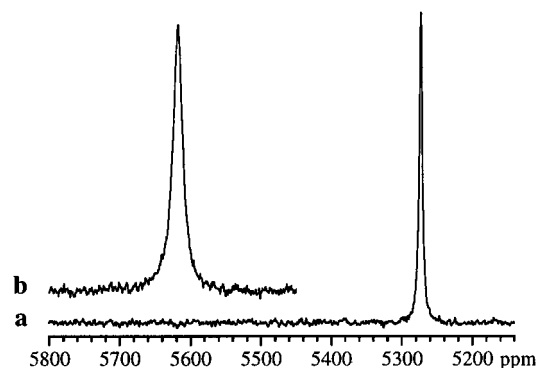

Figure 4. ^{11}B NMR spectrum of $Rb_5Zr_6Cl_{18}B$ dissolved in acetonitrile showing five of the 10 possible isomers of $[(Zr_6C)Cl_{12}Cl_{6-x}(NCCH_3)_x]^{x-5}$, $x = 0-6$.

solvent changes from the Lewis basic $ImCl/AlCl_3$ melt to CH_3CN to the Lewis acidic $ImCl/AlCl_3$ melt, the spectrum undergoes a blue spectral shift (Figure 3). For the three bands shown in the figure, the shift ranges from <1000 cm^{-1} in the mid-visible to 2000 cm^{-1} in the ultraviolet to >2500 cm^{-1} in the near-IR−visible region.

Boron-Centered Clusters. When $Rb_5Zr_6Cl_{18}B$ is dissolved in CH_3CN without addition of another ligand, five singlets are observed (Figure 4): a prominent singlet at 191.2 ppm, and four much less intense singlets at 189, 189.7, 192.1, and 193.8 ppm. Attempts were made to locate a peak for $[(Zr_6B)Cl_{12}(NCCH_3)_6]^{1+}$, but when $TlPF_6$ was added to the cluster containing solution, the boron-centered cluster precipitates completely.

Manganese-Centered Clusters. The MAS solid-state NMR spectrum (7.0 T, 74.67 MHz) for $RbZr_6Cl_{14}Mn$ shows a singlet and its associated spinning side bands centered at 5330 ppm with line width at half-height of approximately 1.7 kHz at spinning rates of 10 and 13 kHz. To calculate the isotropic chemical shift, the spectrum was measured at higher field (8.4 T, 89.65 MHz) at spinning rates of 7.5 and 10.0 kHz. Under these conditions, a cleaner spectrum results and the resonance shifts to 5339 ppm, with line width at half-height of approximately 2.8 kHz. The quadrupole-induced shift $(\delta_{QS}(m))$ to the measured "isotropic" chemical shift for the $m \leftrightarrow \mu - 1$

Spectroscopy of Centered Zr Halide Clusters

J. Am. Chem. Soc., Vol. 119, No. 40, 1997 9453

Figure 5. ^{55}Mn NMR spectra for $[(Zr_6Mn)Cl_{12}L_6]^{5-}$, species (a) an acidic ImCl/AlCl$_3$ melt (L = AlCl$_4^-$) and (b) a basic ImCl/AlCl$_3$ melt (L = AlCl$_4^-$).

transition is given by[29,30]

$$\delta_{QS}(m) = -\frac{3}{40}\left(\frac{e^2qQ}{h\nu_o}\right)^2 \frac{I(I+1) - 9m(m-1) - 3}{I^2(2I-1)^2}\left(1 + \frac{\eta^2}{3}\right)$$

(1)

where (e^2qQ/h) is the nuclear quadrupole coupling constant, ν_o is the Larmor frequency, I is $^5/_2$ for ^{55}Mn, m is $^1/_2$ (only the central transition is observed), and η is the asymmetry parameter of the electric field gradient, which we assumed to be 0. Substitution of data obtained at two field strengths allows calculation of the isotropic ^{55}Mn chemical shift (5359 ppm) and the nuclear quadrupolar coupling constant (5.23 MHz). We have often used Li$_2$Zr$_6$Cl$_{15}$Mn as a solid-state precursor for study of Mn-centered clusters; in the MAS solid-state NMR spectrum of this compound obtained with a 3.0 kHz spinning rate, side bands were unresolved but the broad overlapping multiplet that resulted was centered at approximately 5300 ppm. The manganese environment has O_h symmetry in Li$_2$Zr$_6$Cl$_{15}$Mn and C_{2h} symmetry in RbZr$_6$Cl$_{14}$Mn—we presume that the broader observed line in the former compound reflects local lithium disorder and/or modest lithium substoichiometry (which would necessitate an equal extent of cluster oxidation). When RbZr$_6$-Cl$_{14}$Mn is dissolved in a basic ImCl/AlCl$_3$ (66:34) melt, a singlet at 5618 ppm is observed and in an acidic ImCl/AlCl$_3$ (40:60) melt, the resonance shifts to 5273 ppm (Figure 5). At room temperature, the basic melt is more viscous than the acidic melt and a broader line is observed in the former case (790 Hz vs 250 Hz). Upon heating the basic melt to 70 °C, the line width falls to 200 Hz as the viscosity of the melt decreases, but the line width in the acidic melt increases slightly to 340 Hz. In both the basic and acidic melts we see a modest downfield shift (~10 ppm) when samples were heated to 70 °C (5629 ppm in the basic melt and 5282 ppm in the acidic melt).

Co-, Be-, and N-Centered Clusters. Solid-State Measurements. The MAS solid-state ^{59}Co NMR for Zr$_6$Cl$_{15}$Co shows a singlet centered at 4037 ppm and a width of 780 Hz while spinning at 3.5 kHz in a 7.0 T, 71.21 MHz field. When the sample is spun at 8 and 10 kHz in a 8.47 T, 85.70 MHz field, the singlet shifts to 4051 ppm with the same line width. The isotropic ^{59}Co chemical shift (4082 ppm) and the nuclear quadrupolar coupling constant (9.5 ppm) were computed using eq 1 (I is $^5/_2$ for ^{57}Co, $m = ^1/_2$, $\eta = 0$). In this structure, there is one crystallographically distinct cluster and the cobalt atom sits on a site of rigorous O_h symmetry. We have so far been unsuccessful in attempts to excise clusters with the $[(Zr_6Co)$-

(29) Kyung, H.; Timken, C.; Oldfield, E. *J. Am. Chem. Soc.* **1987**, *109*, 7669–7673.

(30) Samoson, A. *Chem. Phys. Lett.* **1985**, *119*, 29–32.

Table 2. Selected ^{9}Be NMR Data

compound	δ (ppm)	ref
K$_3$Zr$_6$Cl$_{15}$Be	77.1	a
(CH$_3$)$_2$Be·O(C$_2$H$_5$)$_2$	20.8	b
(B$_5$H$_{10}$)$_2$Be	15	b
B$_5$H$_{10}$BeBH$_4$	11.4	b
Be(B$_3$H$_8$)$_2$	4.0	b
Be(NH$_3$)$_4^{2+}$	1.7	c
Be(H$_2$O)$_4^{2+}$	0.0	b, c
BeF$_4^{2-}$	−2	d
(C$_5$H$_5$)$_2$Be	−18.5	e
C$_5$H$_5$BeBH$_4$	−22.1	b

^{a} This work. ^{b} Gaines, D. F.; Coleson, K. M.; Hillenbrand, D. F. *J. Magn. Reson.* **1981**, *44*, 84–88. ^{c} Kovar, R. A.; Morgan, G. L. *J. Am. Chem. Soc.* **1970**, *92*, 5067. ^{d} Kotz, J. C.; Schaeffer, R.; Clouse, A. *Inorg. Chem.* **1967**, *6*, 620. ^{e} Morgan, G. L.; McVicker, G. B. *J. Am. Chem. Soc.* **1968**, *90*, 2789.

Cl$_{12}$]$^{3+}$ core from solid-state precursors and comparison with results from solution cannot be made at this time. The MAS solid-state ^{9}Be spectrum for K$_3$Zr$_6$Cl$_{15}$Be shows a singlet with a width of 130 Hz at 77.1 ppm. This is shifted far downfield from the normal ^{9}Be range (Table 2). T_1 was measured to be 6.4 s for the interstitial Be. Our general experience, as well as electrochemical measurements,[31] show the $\{[(Zr_6Be)Cl_{12}]Cl_6\}^{6-}$ cluster to be a powerful reducing agent and its isolation from solution has been elusive. However, replacement of terminal chlorides with neutral ligands yield a more tractable system and further NMR investigation of such species is underway. Finally, the MAS solid-state ^{15}N NMR spectrum for Zr$_6$Cl$_{15}$N shows a singlet with a width of 66 Hz at 271 ppm. This compares with measured shifts of 163 ppm for $[Fe_6H(N)(CO)_{15}]^{2-}$, 185 ppm for $[(Fe_6N)(CO)_{15}]^{3-}$,[32] 180.2 ppm for $[(Ru_6N)(CO)_{16}]^-$,[33] and 30 ppm for $[(Ru_{10}N)(CO)_{24}]^-$,[34–36] where the latter is a tetracapped octahedron with T_d symmetry. Solution studies for the nitride centered clusters have been undertaken but have been hampered by limited solubility of the cluster precursor and the lower sensitivity of this nucleus.

Discussion

The results given in the preceding section are important for two principal reasons. First, the NMR data given here for the full set of $[(Zr_6Z)Cl^i_{12}L^a_6]^{m-}$ (Z = Be, B, C, N, Mn, Co) molecules are quite without precedent in that that no other series of molecules offers such a variety of nuclei within a single chemical environment. Second, these data demonstrate the analytical usefulness that NMR-active interstitials offer in studies of the solution chemistry of hexanuclear zirconium clusters—both for establishing species present and for information concerning ligand-exchange kinetics. Our discussion begins with the second of these aspects.

Speciation and Ligand Exchange. The most detailed data we have collected to date are for carbon-centered clusters. The chemistry of these systems originates in the essentially quantitative preparation of a solid-state precursor, KZr$_6$Cl$_{15}$C. There

(31) Sun, D.; Hughbanks, T. Unpublished results.

(32) Pergola, R. D.; Bandini, C.; Demartin, F.; Diana, E.; Garlaschelli, L.; Stanghellini, P. L.; Zanello, P. *J. Chem. Soc., Dalton Trans.* **1996**, 747–754.

(33) Blohm, M. L.; Gladfelter, W. L. *Organometallics* **1985**, *4*, 45–52.

(34) Bailey, P. J.; Conole, G. C.; Johnson, B. F. G.; Lewis, J.; McPartlin, M.; Moule, A.; Wilkinson, D. A. *Angew. Chem., Int. Ed. Engl.* **1991**, *30*, 1706–1707.

(35) Bailey, P. J.; Conole, G.; Johnson, B. F. G.; Lewis, J.; McPartlin, M.; Moule, A.; Powell, H. R.; Wilkinson, D. A. *J. Chem. Soc., Dalton Trans.* **1995**, 741–751.

(36) Bailey, P. J.; Conole, G.; Johnson, B. F. G.; Lewis, J.; McPartlin, M.; Moule, A.; Powell, H. R.; Wilkinson, D. A. *J. Chem. Soc., Dalton Trans.* **1995**, 1527.

are two crystallographically unique clusters in the $KZr_6Cl_{15}C$ structure, with C_{2v} and C_{2h} site symmetries.[23] The local structural differences between these two clusters are significant but not dramatic; while the $Zr_6Cl_{12}C$ "core" of the two clusters have nearly identical metrical characteristics, the average zirconium−terminal chloride ($Zr-Cl^a$) distances are 0.035 Å longer for the C_{2h} symmetry cluster. The MAS solid-state spectrum for $KZr_6Cl_{15}C$ shows two peaks separated by approximately 3 ppm. In light of results to be discussed below, it is reasonable to attribute this 3 ppm difference to the difference in charge density on the $Zr_6Cl_{12}C$ cores in $KZr_6Cl_{15}C$.

We have routinely used two solvent systems in our investigations of zirconium cluster chemistry, acetonitrile, and ImCl/$AlCl_3$ ionic liquids. When $KZr_6Cl_{15}C$ is dissolved in a Lewis basic ImCl/$AlCl_3$ (67:33) melt, a sharp singlet at 455.5 ppm is obtained. Since the species present in the basic melt are Im^+, $AlCl_4^-$, and Cl^-,[37] we presume that this singlet can be assigned to $\{[(Zr_6C)Cl_{12}]Cl_6\}^{4-}$, where all terminal ligand sites are occupied by chloride. When this solution is titrated into the Lewis acidic regime by addition of $AlCl_3$ (until the ImCl/$AlCl_3$ ratio is approximately 46:54) a singlet at 471.9 ppm is the only feature observed in the interstitial region of the spectrum. Although speciation in acidic chloroaluminate melts is complicated by the presence of multiple $[Al_nCl_{(3n+1)}]^-$ species, the principal species thought to be present in an ImCl/$AlCl_3$ (46:54) melt are Im^+, $AlCl_4^-$, and $Al_2Cl_7^-$.[37] It is therefore plausible to suppose that in the acidic melt, clusters can be formulated as $\{[(Zr_6C)Cl_{12}](AlCl_4)_6\}^{4-}$, where the cluster is weakly ligated by the strongest base present: $AlCl_4^-$ anions. The same supposition has been made regarding the coordination of analogous $[(Nb,Ta)_6Cl_{12}]^{2+}$ cluster cores in the acidic melt.[19,20]

When $KZr_6Cl_{15}C$ is dissolved in CH_3CN and 6 equiv of PPNCl are added, a singlet corresponding to the $[(Zr_6C)Cl_{18}]^{4-}$ cluster is observed at 457.7 ppm (Figure 1, spectrum a, peak J); differential solvation is apparently responsible for a 2.2 ppm shift for the same cluster species dissolved in the basic ImCl/$AlCl_3$ melt. At the other extreme, when $KZr_6Cl_{15}C$ is dissolved in CH_3CN and 6 equiv of $TlPF_6$ are added to remove the terminal chloride ligands, a sharp singlet at 480.1 ppm and a much less intense singlet at 472.9 ppm are obtained (Figure 1, spectrum d, peaks A and B). We assign the singlet A (480.1 ppm) to the fully solvated, cationic species $\{[(Zr_6C)Cl_{12}](NCCH_3)_6\}^{2+}$, and it is likely that peak B (472.9 ppm) arises from $\{[(Zr_6C)Cl_{12}]Cl(NCCH_3)_5\}^+$. A small amount of the latter species apparently survives, despite the fact that a 2-fold excess of $TlPF_6$ was added. A possible explanation for the observation of a singlet corresponding to the $\{[(Zr_6C)Cl_{12}]Cl(NCCH_3)_5\}^+$ ion is that some sacrificial cluster decomposition occurs to yield some free chloride in excess of added Tl^+ ion.

Having established, at least tentatively, the chemical shifts for the species $[(Zr_6C)Cl_{18}]^{4-}$ and $\{[(Zr_6C)Cl_{12}](NCCH_3)_6\}^{2+}$, NMR evidence for the eight possible intermediate species, $\{[(Zr_6C)Cl_{12}]Cl_{6-n}(NCCH_3)_n\}^{(4-n)-}$ was sought. When $KZr_6Cl_{15}C$ is dissolved in CH_3CN without any added chloride, three singlets are observed (Figure 1, spectrum c): an intense singlet D (466.8 ppm) and two less intense singlets C (470.6 ppm) and B (472.9 ppm). As the labeling indicates, the last of these peaks corresponds to the species we have already assigned as $\{[(Zr_6C)Cl_{12}]Cl(NCCH_3)_5\}^+$. Since KCl is virtually insoluble in acetonitrile (3.2×10^{-5} M), we should expect that the cluster species in this solution should have three or fewer terminal chlorides. This fact, and the obvious progression of chemical

shifts themselves, make it reasonable to assign peak D to either *cis*- or *trans*-$[(Zr_6C)Cl_{12}]Cl_2(NCCH_3)_4$ and to attribute peak C to the other $[(Zr_6C)Cl_{12}]Cl_2(NCCH_3)_4$ isomer. If $KZr_6Cl_{15}C$ is dissolved in acetonitrile that is saturated with NaCl, the NMR spectrum shows five clearly observable singlets (and two very weak "peaks") with chemical shifts ranging from 459 to 467 ppm (labeled as D−H)—peak D corresponding to one isomer of $[(Zr_6C)Cl_{12}]Cl_2(NCCH_3)_4$ as already discussed. Peaks E through H are attributed to the species *fac*- and *mer*-$\{[(Zr_6C)Cl_{12}]Cl_3(NCCH_3)_3\}^{1-}$ and *cis*- and *trans*-$\{[(Zr_6C)Cl_{12}]Cl_4(NCCH_3)_2\}^{2-}$. The signal-to-noise ratio applicable to the weak signals at 463.7 and 458.9 ppm is too low (≤ 3) to draw any firm conclusions as to their "reality" from this experiment; nevertheless, we have attached the label "I" to the peak at 458.9 ppm for reasons indicated below; we believe that this is the signal for $\{[(Zr_6C)Cl_{12}]Cl_5(NCCH_3)\}^{3-}$.

In an effort to gain further support for the peak assignments discussed in the previous paragraph, we carried out an experiment in which 9 equiv of PPh_3 were added to an acetonitrile solution of $KZr_6Cl_{15}C$. One intent of this experiment was to displace bound CH_3CN with phosphines and to exploit any observed $^2J_{P-Zr-C}$ coupling in assigning interstitial ^{13}C signals. The ^{31}P spectrum (Figure 2, inset) shows that the phosphines do appear to bind to zirconium, but no coupling to the interstitial carbon was observed. Although we are presently unable to conclusively assign the four singlets in the ^{31}P spectrum, free PPh_3 and $OPPh_3$ can be ruled out since they would found at −4.6 and 24.8 ppm, respectively. The possibility that some or all of the resonances observed in the ^{31}P spectrum are due to the presence of phosphine or phosphine oxide complexed to other metal centers (eg., $[ZrCl_{6-n}(PPh_3)_n]^{n-6}$) cannot be ruled out. The absence of coupling is in contrast with two-bond couplings seen in mononuclear M−carbonyl−phosphine and −phosphite complexes; typical *trans* $^2J_{P-M-C}$ coupling for group 6 metal−carbonyl−phosphine and −phosphite complexes range from 12 to 45 Hz.[38] In the ^{13}C spectrum, we observed five peaks (Figure 2): an intense singlet at 460.2 ppm and four weaker singlets at 459.0, 461.6, 463.3, and 464.9 ppm. The chemical shifts of each of these resonances closely correspond to resonances observed in spectra recorded in the absence of added phosphine (peaks E−I in Figure 1). The solubility of several PPh_3-substituted species is low; on standing, a cream-colored precipitate forms in the NMR tube and the color of the solution is visibly less intense. It is therefore not surprising that the intensity pattern in Figure 2 differs from the spectra in Figure 1; the most soluble species predominate and these are apparently the more chloride-rich, and therefore anionic, species. In particular, the resonance at 459 ppm that is clearly observable in this experiment buttresses our assignment of the resonance at the same frequency (I) in Figure 1. What is perhaps surprising is that replacement of CH_3CN by PPh_3 would be accompanied by so little change in chemical shift of the interstitial carbide. Thus, two interpretations are possible: either the phosphine substituted clusters have ^{13}C chemical shifts that are very close to those of CH_3CN-substituted clusters *or* some cluster decomposition occurs to yield mononuclear Zr^{IV} ions that serve to competitively scavenge all the added phosphine and the complexes formed in this process serve as counterions in precipitating some of the $\{[(Zr_6C)Cl_{12}]Cl_{6-n}(NCCH_3)_n\}^{(4-n)-}$ species. In light of this ambiguity, work is underway using phosphines with more modest steric requirements; the large PPh_3 cone angle may prevent its binding to the cluster. In support of this hypothesis, preliminary experiments with ^{11}B-centered

(37) Fannin, A. A., Jr.; Floreani, D. A.; King, L. A.; Landers, J. S.; Piersma, B. J.; Stech, D. J.; Vaughn, R. L.; Wilkes, J. S.; Williams, J. L. *J. Phys. Chem.* **1984**, *88*, 2614−2621.

(38) Braterman, P. S.; Milne, D. W.; Randall, E. W.; Rosenberg, E. *J. Chem. Soc., Dalton Trans.* **1973**, 1027−1031.

clusters show definitive $^{31}P-^{11}B$ coupling when smaller phosphines are bound.

Chemical shifts for all 10 possible $\{[(Zr_6C)Cl_{12}]Cl_{6-n}(NCCH_3)_n\}^{(4-n)-}$ species have been observed and span the range 457.7−480.1 ppm. Although assignments of the resonances in the middle of the range is tentative, assignments at the extremes seem assured. It is clear that as fewer chlorides are bound to the cluster and the total charge decreases from −4 to +2, the interstitial becomes more deshielded. (The extent to which the more highly charged species are engaging in ion-pairing in CH_3-CN has not yet been addressed.) The net cluster charge is the dominant factor influencing relative chemical shifts observed within a series of cluster species, but ligand substitution patterns (i.e., *cis* vs *trans* and *fac* vs *mer*) also have a significant effect. The chemical shift for the carbide carbon in the basic ImCl/$AlCl_3$ melt is reasonably close to that obtained for $[(Zr_6C)Cl_{18}]^{4-}$ in acetonitrile. Assuming that the cluster species in the acidic melt is $[(Zr_6C)Cl_{12}(AlCl_4)_6]^{4-}$, we can see that little of the charge on the $(AlCl_4)^-$ ion is transferred to the cluster since the observed chemical shift is comparable to that of the $\{[(Zr_6C)-Cl_{12}]Cl(NCCH_3)_5\}^+$ in acetonitrile.

The ligand exchange kinetics of the carbide-centered cluster were briefly examined using ^{13}C NMR. In this experiment, some labeled CH_3*CN was added to the solution to enhance the signal from CH_3CN bound to the cluster. Spectra were identical at −30 and 20 °C, showing singlets at 132.8 and 132.1 ppm for the cluster-bound acetonitrile. However, at 30 °C the two signals from bound acetonitrile disappear. On the other hand, the region between 455 and 470 ppm remained nearly unchanged from −30 to 70 °C. These results indicate that CH_3-CN exchange is slow on the solvated clusters, with a coalescence temperature between 20 and 30 °C and that Cl^- exchange is extremely slow, with a coalescence temperature greater than 70 °C. Since the steric environment around zirconium in a cluster is considerably more congested than, say, a mononuclear octahedral complex, we assume that exchange occurs by a primarily dissociative mechanism. Operating under that assumption, we further assume a simple Arrhenius expression for the rate constant, $k_T = A \exp(-E_a/RT)$, for which A is on the order of 1×10^{15} (a reasonable value for mononuclear complexes for which a dissociative mechanism is indicated).[39] Peak positions and widths appear unchanged on moving from 25 to 70 °C so we assume that the terminal chloride exchange rate at 70 °C is slow on a time scale determined by the most closely spaced singlets in the spectrum (63 Hz): $k_{70} \ll 63$ s^{-1}. If we estimate that $k_{70} \leq 1.0 \ s^{-1}$, then we obtain $E_a \geq 100$ kJ mol^{-1} and $k_{25} \leq 3 \times 10^{-3} \ s^{-1}$ for chloride loss.

Though it is implicit in the results discussed to this point, it is worth noting that there is no evidence that interstitial atoms ever exchange with atoms in the environment. This is most directly seen for C-centered clusters that are synthesized with ^{13}C-enriched carbon and for which NMR signal intensity never declines over time in a manner consistent with such exchange (with unenriched solvents, reagents, etc.). On the other hand, we have observed cluster decomposition by monitoring the appearance of product resonances as this decomposition occurs (e.g., when $K_3Zr_6Cl_{15}Be$ is dissolved into deoxygenated water, one observes the growth of a resonance for $Be(H_2O)_4^{2+}$ as the clusters in solution are hydrolyzed).[40]

The electronic spectra of $[(Zr_6C)Cl_{12}L_6]^{m-}$ species have been measured in CH_3CN and in the ImCl/$AlCl_3$ melts and yield an interesting comparison with the NMR results. As the solvent changes from the Lewis basic ImCl/$AlCl_3$ melt to CH_3CN to

Table 3. Selected ^{11}B NMR Data for Boron-Centered Octahedral Clusters

compound	δ, (ppm)	ref
trans-[Fe$_4$Rh$_2$(CO)$_{16}$B]PPN	211	a
cis-[Fe$_4$Rh$_2$(CO)$_{16}$B]PPN	205	a
[Ru$_6$(CO)$_{17}$B]$^-$	196	b
[Ru$_6$(CO)$_{17}$B{AuP(C$_6$H$_4$Me-2)$_3$}]	195	c
HRu$_6$(CO)$_{17}$B	194	b
[Ru$_6$(CO)$_{17}$B{AuPPh$_3$}]	194	c
[Ru$_6$(CO)$_{16}$B{AuPPh$_3$}]	194	c
[Ru$_6$H(CO)$_{16}$B{AuP(C$_6$H$_4$Me-2)$_3$}]	194	c
[Ru$_6$H(CO)$_{16}$B{AuPPh$_3$}]	193	c
[(Zr$_6$B)Cl$_{18-x}$(NCCH$_3$)$_x$]$^{x-5}$	193.8, 192.1, 191.3	d
	189.8, 189.0	d
Rb$_5$Zr$_6$Cl$_{18}$B (solid)	187	e
[Zr$_6$Cl$_{18}$B]$^{5-}$ in CH$_3$CN	185	f
[Zr$_6$Cl$_{18}$B]$^{5-}$ in ImCl/AlCl$_3$	184	e

^{a} Khattar, R.; Puga, J.; Fehlner, T. P.; Rheingold, A. L. *J. Am. Chem. Soc.* **1989**, *111*, 1877−1879. ^{b} Hong, F.-E.; Coffy, T. J.; McCarthy, D. A.; Shore, S. G. *Inorg. Chem.* **1989**, *28*, 3284. ^{c} Housecroft, C. E.; Matthews, D. M.; Waller, A.; Edwards, A. J.; Rheingold, A. L. *J. Chem. Soc., Dalton Trans.* **1993**, 3059−3070. ^{d} This work. ^{e} Tian, Y.; Hughbanks, T. *Inorg. Chem.* **1995**, *34*, 6250−6254. ^{f} Tian, Y. Ph.D. Thesis, Texas A&M University, 1995.

the Lewis acidic ImCl/$AlCl_3$ melt, the spectrum undergoes a blue shift by as much as 2500 cm^{-1} (Figure 3), while the ^{13}C resonance for the interstitial shifts downfield from 455.5 ppm to 471.9 ppm in the different solvents. From the NMR data we know that the species in the basic melt is $[(Zr_6C)Cl_{18}]^{4-}$, in CH_3CN is a mixture of $[(Zr_6C)Cl_{13}(NCCH_3)_5]^{1+}$ and $[(Zr_6C)-Cl_{14}(NCCH_3)_4]$ and in the acidic melt is $[(Zr_6C)Cl_{12}(AlCl_4)_6]^{2-}$. We ascribe this spectral shift to the change in charge on the cluster and to the shifting of molecular orbitals as a result of the change of ligands. Molecular orbital calculations are consistent with a similar blue spectral shift observed for the iron-centered cluster.[41] In addition, each of the three bands seem to be affected by the change in charge and ligands differently, and as mentioned above, $AlCl_4^-$ does not seem to donate much of its charge to the cluster, which is apparent from the similarities between the spectra with the cluster dissolved in acetonitrile and the acidic melt.

The speciation exhibited by carbide-centered clusters is paralleled by the boron-centered systems. When Rb$_5$Zr$_6$Cl$_{18}$B is dissolved in CH_3CN without adding any additional source of Cl^-, five singlets are observed (189, 189.7, 191.2, 192.1, and 193.8 ppm; Figure 4). The peak at 191.2 ppm dominates, with the others being much less intense. Since chloride exchange is slow (recall the ^{13}C NMR variable-temperature results), this implies that there is solvolysis of the cluster in solution and that some RbCl (solubility in acetonitrile is 3.0×10^{-4} M)[42] must precipitate during dissolution. As for the carbide-centered cluster, each of the singlets represent one of the $[(Zr_6B)Cl_{12}Cl_{6-n}(NCCH_3)_n]^{n-5}$ species. The cluster can be driven to the fully anated $[(Zr_6B)Cl_{12}Cl_6]^{5-}$ species in CH_3CN (185 ppm) if extra anions are provided.[43] We were unable to measure a resonance for $[(Zr_6B)Cl_{12}(NCCH_3)_6]^{1+}$, since the cluster precipitates completely upon the addition of TlPF$_6$. When the boron-centered cluster precursor is dissolved in the basic molten salt, a singlet at 184 ppm is obtained for the fully anated $[Zr_6Cl_{18}B]^{5-}$.[7] Chemical shifts for the B-centered cluster are quite comparable to those for other boron-centered metal clusters (Table 3).

The ^{55}Mn chemical shift change observed on moving from the basic melt to the acidic melt is in the opposite direction to

(39) Wilkins, R. G. *Kinetics and Mechanism of Reactions of Transition Metal Complexes*; 2 ed.; VCH: New York, 1991.

(40) Xie, X. B.; Sun, D.; Hughbanks, T. Unpublished results.

(41) Hughbanks, T. *J. Alloys Compd.* **1995**, *229*, 40−53.

(42) Stephen, H.; Stephen, T. *Solubilities of Inorganic and Organic Compounds*; Stephen, H.; Stephen, T., Ed.; Pergamon Press Limited: Oxford, 1963.

(43) Tian, Y. Ph.D. Thesis, Texas A&M University, 1995.

that observed for ^{13}C- and ^{11}B-centered clusters. In the latter cases, the resonances shift upfield in the basic melt, where the terminal ligands are presumed to be chlorides. For the manganese-centered cluster the resonance is shifted upfield in the *acidic* melt, where the terminal ligand positions are likely to be occupied by very weakly coordinating tetrachloroaluminate ions. We comment briefly on these opposing trends below. It would be enlightening to have compared the results for Mn-centered clusters with those for another NMR-active transition metal-centered cluster to determine whether this reversal is unique to manganese. Unfortunately, our inability to find a solvent suitable for excising Co-centered clusters from solid-state precursors has prevented us from making such a comparison.

Physical Implications. The chemical shifts exhibited by interstitials in clusters are quite generally outside the range exhibited by "ordinary" diamagnetic molecules. For carbide-, boride-, and nitride-centered carbonyl-ligated clusters of the later transition metals, such exceptional chemical shifts have been observed and have received some theoretical analysis. As we have seen, some of our chemical shift data for such interstitials is quite comparable to data for carbonyl clusters. Virtually all qualitative discussion of chemical shifts in these systems has begun with Ramsey's expression and focused on the paramagnetic term (σ_p):[44,45]

$$\sigma = \sigma_d + \sigma_p \tag{2}$$

$$\sigma_p^\alpha(Z) = -$$

$$\frac{\mu_0 e^2}{8\pi m^2} \sum_{k \neq 0} \frac{\langle 0|\sum_i L_{i\alpha}|k\rangle\langle k|\sum_i \frac{L_{i\alpha}}{r_Z^3}|0\rangle + \langle 0|\sum_i \frac{L_{i\alpha}}{r_Z^3}|k\rangle\langle k|\sum_i L_{i\alpha}|0\rangle}{E_k - E_0} \tag{3}$$

where Z is the nucleus under consideration, α runs over the Cartesian coordinates, k runs over all excited states, and i runs over all the electrons. The paramagnetic contribution to shielding arises from the second-order mixing of paramagnetic excited states into the ground state by the applied magnetic field.[46] Of course, all of our data are compared to standards for the respective elements involved and this fact alone means that our conclusions must at this stage be purely qualitative.

Let us first turn our attention to the main group interstitial atoms: beryllium, boron, carbon, and nitrogen. Qualitatively, trends in paramagnetic contributions to the chemical shift depend on three factors:[47,48] (a) the effective p orbital radii, via the $\langle 1/r^3 \rangle$ dependence in eq 2, (b) the magnitude of the interstitial p orbital contributions to the molecular orbitals involved in the ground to excited state excitations and orbital symmetries—which defines the *significant* excited states, and (c) energy gaps between the ground and significant excited states, via the $(1/\Delta E)$ dependence.

The chemical shift trends on moving through the Be → N series show the combined effects of the three effects listed above. We expect, of course, that the p orbital radii decline through the series and structural data (Zr–Z distances: Z = Be, 2.333 Å; Z = B, 2.317 Å; Z = C, 2.279 Å; Z = N, 2.273

Å)$^{21-24}$ show that this is the case. Spectroscopic (calculated) values of $\langle a_0^3/r^3 \rangle_{2p}$ for the free atoms show a more pronounced variation: B, 0.608 (0.773); C, 1.23 (1.68); N, 2.46 (interpolated) (3.09).[49,50] However, the magnitude of the chemical shift change on moving from Be to C seems to be larger than can be accounted for by the change in orbital radii and the ^{15}N shift seems to be smaller than that observed for ^{13}C-centered clusters (careful comparisons are unfortunately precluded by difficulties in accounting for differences in the reference compounds). These facts can be explained only by consideration of Zr–Z bonding in the clusters. The O_h symmetry of the clusters means that molecular orbitals in the t_{1u} manifold are the only ones that have both significant Z character and have nonzero angular momentum. As has been pointed out by Khattar and Fehlner,[47,48] the matrix elements that make the largest contributions to σ_p are those where the interstitial p orbital contributions at "both ends" of the excitations (occupied and unoccupied orbitals) in eq 3 are significant.

Both ^{13}C and ^{11}B chemical shifts respond to changes in cluster charge in the same manner (cationic species show greater deshielding) and move over a similar range on moving from $\{[(Zr_6Z)Cl_{12}](NCCH_3)_6\}^{y+}$ to $\{[(Zr_6Z)Cl_{12}]Cl_6\}^{(6-y)-}$: ~23 ppm for ^{13}C ($y = 2$) and ~10 ppm for ^{11}B ($y = 1$). The electronic "damping" and charge delocalization provided by the (Zr_6Z)-Cl_{12} environment is evident since the ranges over which the chemical shift moves are modest. The small effect that exo-ligand basicity exerts on the electronic spectra has been noted in our previous work.[4,6,10] As our earlier discussion indicated, we do not know whether PPh$_3$ even binds to the C-centered cluster. Assuming phosphines *can* be bound to the cluster, the octahedral environment of the interstitial carbide will undoubtedly have an important effect on the magnitude of the $^2J_{P-Zr-C}$ coupling. There will be no interstitial s–p mixing because s and p orbital contributions to Zr–Z bonding are respectively restricted to orbitals of a_{1g} and t_{1u} symmetry. The a_{1g} orbital possessing carbon 2s character (**2**) lies roughly 10 eV lower in energy than those with significant Zr–P bonding character and there is very little phosphorus 3s–carbon 2s coupling provided by the intervening cage orbitals. In contrast, the principal σ donor orbital of a carbonyl ligand incorporates significant s–p hybridization and lies fairly close in energy to the phosphine lone pair orbital—and is thus coupled to the phosphine orbital via intervening metal orbitals in mononuclear complexes. If this explanation is correct, we may have a greater chance of observing ^{31}P–Z coupling for Z = ^{11}B and ^{9}Be since these atoms' s orbitals lie closer in energy to the phosphine lone pair. (The Be atom ionization energy is 9.3 eV,[51] close to the lone pair ionization energy of PR$_3$ molecules—typically 8–9 eV.)[52]

2 a_{1g}
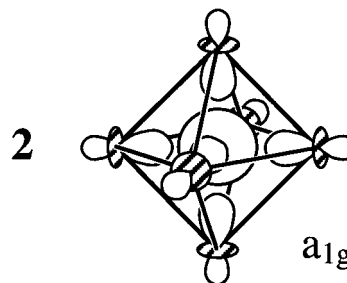
(44) Ramsey, N. F. *Phys. Rev.* **1950**, *78*, 699−703.

(45) Mason, J. *Multinuclear NMR*; Mason, J., Ed.; Plenum: New York, 1987.

(46) Griffith, J. S.; Orgel, L. E. *Trans. Faraday Soc.* **1957**, *53*, 601−606.

(47) Fehlner, T. P.; Czech, P. T.; Fenske, R. F. *Inorg. Chem.* **1990**, *29*, 3103−3109.

(48) Khattar, R.; Fehlner, T. P.; Czech, P. T. *New J. Chem.* **1991**, *15*, 705−711.

(49) Huzinaga, S. *Gaussian Basis Sets for Molecular Calculations*; Huzinaga, S., Ed.; Elsevier: Amsterdam, 1984.

(50) Barnes, R. G.; Smith, W. V. *Phys. Rev.* **1954**, *93*, 95−98.

(51) Moore, C. E. Atomic energy levels. NBS Circular 467, 1970.

(52) Hillier, I. H.; Saunders, V. R. *Chem. Commun.* **1970**, 316−318.

Table 4. Comparison of Selected ^{55}Mn and ^{59}Co Data

ref	Mn Compound	δ, (ppm)	δ, (ppm)	Co Compound	ref
a	MnH(PF$_3$)$_5$	-2953	-3900	CoH(PF$_3$)$_4$	*i*
b	[Mn(CO)$_5$]$^-$	-2780	-3090	[Co(CO)$_4$]$^-$	*i*
a, b	MnH(CO)$_5$	$-2630/-2578$	-3700	CoH(CO)4	*i*
b, c	MnCp(CO)$_3$	-2225 to -2280	-2670	CoCp(CO)$_2$	*i*
c−e	Mn$_2$(CO)$_{10}$	-2227 to -2331	-2100	Co$_2$(CO)$_8$	*i*
f	Mn(CO)$_5$Co(CO)$_4$	-1840	2900	Mn(CO)$_5$Co(CO)$_4$	*f*
c, d	[Mn(CO)$_6$]$^+$	-1445	0	[Co(CN)$_6$]$^{3-}$	*j*
g	MnO$_4$$^-$	0	1300	[Co(CNO)$_6$]$^{3-}$	*k*
c	*fac*-[Mn(CO)$_3$(NCMe)$_3$]$^+$	490	4082	Zr$_6$Cl$_{15}$Co	*h*
h	RbZr$_6$Cl$_{14}$Mn	5359	4880	[Co(dmg)$_3$]	*k*
h	[(Zr$_6$Mn)Cl$_{12}$(AlCl$_4$)$_6$]$^{5-}$	5273	6620	[Co(bipy)$_3$]$^{3+}$	*l*
h	Li$_2$Zr$_6$Cl$_{15}$Mn	5330	7130	[Co(phen)$_3$]$^{3+}$	*j*
h	[(Zr$_6$Mn)Cl$_{18}$]$^{5-}$	5618	7144	[Co(en)$_3$]$^{3+}$	*l, m*
			8173	[Co(NH$_3$)$_6$]$^{3+}$	*j, k, m*
			14100	[Co(CO$_3$)$_3$]$^{3-}$	*j*
			15100	[Co(H$_2$O)$_6$]	*n*

^{a} Miles, W. J. J.; Garrett, B. B.; Clark, R. J. *Inorg. Chem.* **1969**, *8*, 2817−2818. ^{b} Calderazzo, F.; Lucken, E. A. C.; Williams, D. F. *J. Chem. Soc. (A)* **1967**, 154−158. ^{c} Rehder, D.; Bechthold, H.-C.; Kececi, A.; Schmidt, H.; Siewing, M. *Z. Naturforsch.* **1982**, *37 b*, 631−645. ^{d} Kececi, A.; Rehder, D. *Z. Naturforsch.* **1981**, *36B*, 20−26. ^{e} Onaka, S.; Miyamoto, T.; Sasaki, Y. *Bull. Chem. Soc. Jpn.* **1971**, *44*, 1851−1854. ^{f} Mooberry, E. S.; Sheline, R. K. *J. Chem. Phys.* **1972**, *56*, 1852−1855. ^{g} Gudlin, D.; Schneider, H. *J. Magn. Reson.* **1975**, *17*, 268−271. ^{h} This work. ^{i} Lucken, E. A. C.; Noack, K.; Williams, D. F. *J. Chem. Soc. (A)* **1967**, 148−154. ^{j} Yamasaki, A.; Yajima, F.; Fujiwara, S. *Inorg. Chim. Acta* **1968**, *2*, 39−42. ^{k} Juranic, N. *Inorg. Chem.* **1983**, *22*, 521−525. ^{l} Dharmatti, S. S.; Kanekar, C. R. *J. Chem. Phys.* **1959**, *31*, 1436−1437. ^{m} Doddrell, D. M.; Bendall, M. R.; Healy, P. C.; Smith, G.; Kennard, C. H. L.; Raston, C. L.; White, A. H. *Aust. J. Chem.* **1979**, *32*, 1219−1230. ^{n} Navon, G. *J. Phys. Chem.* **1981**, *85*, 3547−3549.

Considering the close correspondence between chemical shifts of {[(Zr$_6$B,C)Cl$_{12}$](L)$_6$}$^{m-}$ clusters and B- or C-centered carbonyl clusters of the later transition metals (Tables 1 and 4), the differences we observe for N-centered clusters is inexplicable. All of the reported NMR data for carbide- and boride-centered octahedral metal clusters falls inside 77 and 27 ppm ranges, respectively. These ranges are well downfield from those of the "normal" ^{13}C and ^{11}B regions. In addition, the chemical shift seems to be more strongly influenced by the geometry of the cage surrounding the interstitial (e.g., octahedral vs trigonal prismatic) than by the identity of the metals that constitute the cage. Although Mason has correlated the chemical shifts of different main group-centered clusters with size of the interstitial cavity,[53,54] we see no such correlation in our Zr$_6$ cluster data; this is despite the fact that our ^{13}C and ^{11}B data show chemical shifts are in the range found for late-transition metal octahedral clusters. Kaupp has used density-functional (DFT) calculations to obtain theoretical chemical shift tensors for a series of C-centered transition metal clusters with carbonyl ligands.[55] He concludes that shifts of excited states and the cluster "band gaps" have the most direct effect on the paramagnetic contribution to the observed chemical shift and that, other factors being equal, compression of the interstitial cavity would not be expected to cause increased deshielding.[55] The DFT predictions are well supported by experimentally determined chemical shift anisotropy measurements.[56] The ^{15}N nucleus in the zirconium cluster is considerably more deshielded (271 ppm) than in the [Fe$_6$H(N)(CO)$_{15}$]$^{2-}$ (163 ppm) and [(Fe$_6$)N)(CO)$_{15}$]$^{3-}$ (185 ppm) clusters reported by Pergola and co-workers[32] and [(Ru$_6$)(N)(CO)$_{16}$]$^-$ (180 ppm) reported by Blohm and Gladfelter.[33] Without data on more systems, further analysis seems fruitless.

The chemical shifts observed for ^{55}Mn- and ^{59}Co-centered clusters are at least an order of magnitude larger than observed for clusters centered by p block elements. To our knowledge, there are no ^{55}Mn and ^{59}Co NMR measurements for compounds that are chemically comparable to the clusters investigated here.

Comparison with other ^{55}Mn chemical shifts (Table 4) shows that the Mn-centered clusters under investigation here exhibit deshielding that greatly exceeds that found in any previously reported manganese compounds. These unprecedented chemical shifts clearly reflect the fact that the manganese chemical environment in hexanuclear zirconium clusters is unlike any molecules for which ^{55}Mn NMR spectra have so far been measured. In contrast, the ^{59}Co shifts presented here are quite within the range of chemical shifts measured for mononuclear low-spin Co^{III} complexes. Further discussion of the origin of chemical shifts and comparison with previously measured shifts follows.

The large ranges over which chemical shifts vary for cobalt and manganese is understood to result from large induced paramagnetic contributions that are in turn characteristic of transition metal compounds where low-lying d manifold excited states are accessible. For example, studies of Co^{III} (d^6) complexes show a clear qualitative correlation between chemical shift, temperature-independent paramagnetism (TIP), and ligand field strength.[57−64] This correlation can be seen in Table 4 where the weak field (but still low-spin) hexaaquo complex, [Co(H$_2$O)$_6$]$^{3+}$, stands at the deshielded extreme of the known chemical shift range. Of course, the hexaaquo ion occupies a position near the high-spin to low-spin crossover point as a function of ligand field strength and therefore possesses very low-lying paramagnetic excited states. Likewise, the relationship between TIP and low-lying excited states of the MnO$_4$$^-$ ion is well established,[65,66] and the permanganate ion stands

(53) Mason, J. *J. Am. Chem. Soc.* **1991**, *113*, 24−26.
(54) Mason, J. *J. Am. Chem. Soc.* **1991**, *113*, 6056−6062.
(55) Kaupp, M. *Chem. Commun.* **1996**, 1141−1142.
(56) Heaton, B. T.; Iggo, J. A.; Longoni, G.; Mulley, S. *J. Chem. Soc., Dalton Trans.* **1995**, 1985−1989.

(57) Lucken, E. A. C.; Noack, K.; Williams, D. F. *J. Chem. Soc. (A)* **1967**, 148−154.
(58) Mooberry, E. S.; Sheline, R. K. *J. Chem. Phys.* **1972**, *56*, 1852−1855.
(59) Yamasaki, A.; Yajima, F.; Fujiwara, S. *Inorg. Chim. Acta* **1968**, *2*, 39−42.
(60) Juranic, N. *Inorg. Chem.* **1983**, *22*, 521−525.
(61) Dharmatti, S. S.; Kanekar, C. R. *J. Chem. Phys.* **1959**, *31*, 1436−1437.
(62) Doddrell, D. M.; Bendall, M. R.; Healy, P. C.; Smith, G.; Kennard, C. H. L.; Raston, C. L.; White, A. H. *Aust. J. Chem.* **1979**, *32*, 1219−1230.
(63) Weiss, R.; Verkade, J. G. *Inorg. Chem.* **1979**, *18*, 529−530.
(64) Navon, G. *J. Phys. Chem.* **1981**, *85*, 3547−3549.
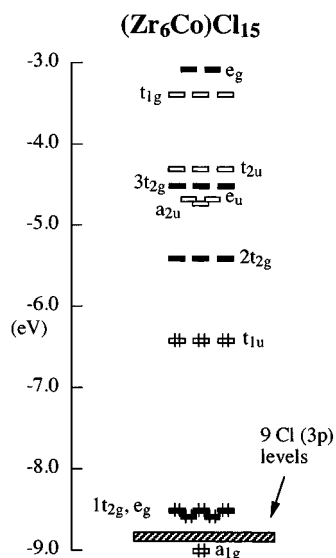(65) Carrington, A. *Mol. Phys.* **1960**, *3*, 271−275.
(66) Jorgensen, C. K. *Prog. Inorg. Chem.* **1970**, *12*, 101−158.

(Zr₆Co)Cl₁₅

Figure 6. Molecular orbital diagram for $(Zr_6Co)Cl_{15}$, with the e_g and t_{2g} sets of orbitals highlighted.

near the extreme in the known manganese chemical shift range.

Interestingly, while the ^{59}Co chemical shift we observe for $[(Zr_6Co)Cl_{15}]$ is quite ordinary within the context of shifts measured for mononuclear Co^{III} (d^6) complexes, the ^{55}Mn shifts we have recorded for $[(Zr_6Mn)Cl_{12}]L_6$ clusters lie more than 4000 ppm outside of the range established in all previously measured manganese compounds. This difference is seen despite the fact that a series of isoelectronic analogs for the two metals have similar chemical shifts (see Table 4). Oddly enough, this disparity highlights the differences between the two metals in the chemistry of their *mononuclear* d^6 complexes. While low-spin Co^{III} complexes are in abundant supply, strong field ligands are required to stabilize the Mn^I oxidation state (e.g., carbonyls and organometallics); the series of low-spin Mn^I complexes that one might imagine would exhibit highly deshielded NMR signals simply do not exist because they are likely to disproportionate.

A rigorous treatment of the origin of chemical shifts in molecules such as these poses a stiff challenge for contemporary computational theory. Still, we can identify some of the most important electronic factors that are likely to contribute to the paramagnetic shift. Following on the analysis of main group-centered clusters, the most important contributing excited states should meet two criteria: (a) the $\langle 1/r^3 \rangle$ dependence and constraint of nonzero angular momentum will heavily weight excitations involving the promotion of electrons both *to* and *from* cluster orbitals with significant interstitial d character (e_g or t_{2g}); (b) the symmetry of the interstitial atom **L** operator constrains the excited states to be of T_{1g} symmetry. These two constraints serve to limit primary consideration to $^1T_{1g}$ states derived from four possible orbital excitations, as explained below. (The same considerations applied to low-spin mono-nuclear Co^{III} complexes allowed Griffith and Orgel to correlate TIP with the energy of the lowest lying $^1T_{1g}$ excited state.)[46] These four excitations can be identified by reference to the molecular orbital diagram given in Figure 6, derived from Γ point ($k = 0$) calculation on one cubic net from $[(Zr_6Co)Cl_{15}]$ using a DFT calculation (computational details are given in the Appendix). The diagram includes bonding and antibonding orbitals localized on the Zr$_6$Co cage and within a ± 3 eV range of the Fermi level.

Bonding in hexanuclear clusters has been the subject of numerous studies, so we will give only a brief summary of the salient features of Figure 6. This calculation, like previously

reported extended Hückel calculations on $[(Zr_6M)X_{18}]$ clusters (M = transition metal, X = halide),[41,67,68] yields nine cage-localized bonding orbitals—consistent with the observed chemical preference these systems show for the 18 e$^-$ count. The symmetries and energetic ordering of these bonding levels is also generally consistent with previous EH results ($a_{1g} < t_{2g} \sim e_g < t_{1u}$). The a_{1g} orbital is a bonding combination of the lowest energy Zr$_6$ cage orbital and the Co 4s orbital (as in **2**). The e_g orbital set consists primarily of the e_g symmetry d orbitals on Co (with some stabilization provided by bonding to the Zr$_6$ cage) while the t_{1u} orbitals (the degenerate HOMO) are almost entirely localized on the Zr$_6$ cage (and is little stabilized by mixing with the Co 4p orbitals). Finally, the t_{2g} orbital set is a bonding combination of the Co d(t_{2g}) set and two Zr$_6$ cage orbitals of like symmetry.

Mixing among t_{2g} orbitals is important in determining the final energetic disposition of both bonding and antibonding (unoccupied) orbitals that influence the chemical shift. Illustration **3** schematically shows how this mixing occurs. The two Zr$_6$ cage orbitals are respectively Zr—Zr bonding (t_{2g}) and antibonding (t_{2g}*) combinations that have counterparts in the well-known *vacant* clusters of niobium and tantalum $[(Nb,Ta)_6X_{12}L_6]$.[68–70] There is a closer energy match and larger overlap between the Co d(t_{2g}) orbitals and the bonding Zr$_6$(t_{2g}) orbitals and consequently the interaction between these two orbitals dominates the splitting seen in **3**. The three t_{2g} sets of
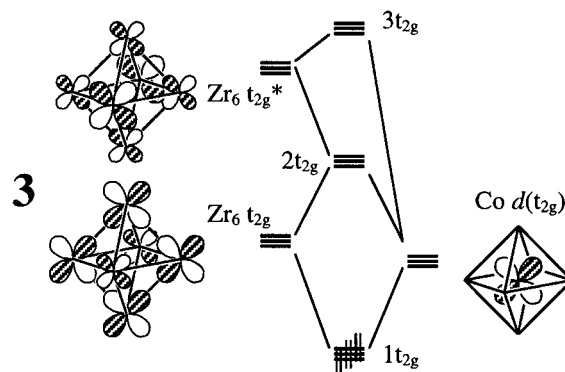
orbitals and the occupied e_g orbital (highlighted in Figure 6) should be key determinants of the chemical shift in both Co- and Mn-centered clusters. Four $^1T_{1g}$ states derived from excitations involving these orbitals should be important: $e_g \rightarrow 2t_{2g}, 3t_{2g}; 1t_{2g} \rightarrow 2t_{2g}, 3t_{2g}$. Charge-iterative extended Hückel calculations reveal no large differences in the energy of these excitations when comparing the cobalt and manganese cases; further work using density-functional methods are underway.

Finally, we return to the curious behavior exhibited by ^{55}Mn-centered clusters when they are moved from a strongly coordinating basic ImCl/AlCl$_3$ molten salt to a very weakly coordinating acidic melt. Not only does the ^{55}Mn resonance move to a more deshielded position in the basic melt, it moves as much as 345 ppm. As we have noted, this shift is in a sense opposite that shown by ^{11}B- or ^{13}C-centered clusters where the shifts are expected responses to increased molecular charge. It seems that the most likely explanation for this behavior derives from orbital energy shifts that affect the paramagnetic contribution to the chemical shift. For example, if there is an average contraction of the cluster dimensions when weakly coordinating

(67) Corbett, J. D. *Pure Appl. Chem.* **1992**, *64*, 1395−1408.

(68) Hughbanks, T. In *Inorganometallic Chemistry*; Fehlner, T. P., Ed.; Plenum Press: New York, 1992; pp 289−331.

(69) Cotton, F. A.; Haas, T. E. *Inorg. Chem.* **1964**, *3*, 10−17.

(70) Bursten, B. E.; Cotton, F. A.; Stanley, G. G. *Isr. J. Chem.* **1980**, *19*, 132−142.

ligands are bound, we would expect bonding−antibonding gaps to increase as the metal−metal bonding is strengthened—this would be expected to lead to destabilization of excited states and a net decrease in deshielding. Extended Hückel calculations show that the molecular orbitals around the HOMO and LUMO shift in energy when the cluster has $AlCl_4^-$ bound at the axial positions vs that of Cl^-.[7] This shift would also account for the change in the electronic spectrum observed for the carbide-centered cluster.

Conclusions

This and other work that is either underway or completed in our laboratory[4−10] makes it clear that zirconium halide cluster chemistry can be fruitfully developed with solid-state cluster compounds serving as the cluster precursors. Direct comparison of NMR spectra for C-, Mn-, and B-centered[7,43] clusters show that such species are excised intact from the solids, and illuminate the changes in cluster environment that ensues in the process. In some cases, there are indications of cluster degradation in this process—but ongoing research indicates that even where degradation occurs, NMR data are invaluable in exposing it.[40] Of course, there is no reason that such solid state−solution comparisons cannot be made for any other Z-centered clusters.

Chemical shifts or shift ranges have now been established for almost all of the centered zirconium chloride clusters $[(Zr_6Z)Cl_{12}(L)_n]^{m-}$. For $[(Zr_6C)Cl_{12}Cl_{6-n}(L)_n]^{n-4}$ ($n = 0−6$ and $L = CH_3CN$ or PPh_3), the ^{13}C chemical shift for the 10 possible species range over 22 ppm, while the charge on the cluster varies from $+2$ to $−4$. For the boron-centered cluster, the range extends over at least 10 ppm, and the range for the manganese-centered cluster is much larger, at least 461 ppm. Furthermore, chemical shifts have also been measured for Be-, N-, and Co-centered clusters.

Now that the chemical shifts have been located, the centered zirconium chloride clusters offer the advantage of NMR characterization of the species over that of the more extensively studied $[\{(Ta,Nb)_6Cl_{12}\}L_6]^{m-}$ and $[\{(Mo,W)_6Cl_8\}L_6]^{m-}$ clusters. With time and more data, NMR should become a valuable and routine tool for determining composition and cluster charge of hexanuclear zirconium clusters.

Appendix. The calculations on which Figure 6 is based were carried out using the DSolid program within the Insight II (Biosym/MSI) suite of programs. DSolid uses a single *k* point ($k = 0$), and the results will not reflect the band dispersion that would be found in a complete band structure calculation on $[(Zr_6Co)Cl_{15}]$. Experience with linked-cluster solids demonstrates that for most metal−metal bonding levels, such dispersion is modest (usually $\sim$ 0.1−0.2 eV or less) in a solid with $Zr−Cl^{a−a}−Zr$ linkages between clusters. In the same spirit, we simplified the calculation by inclusion of only one of the two interpenetrating networks that make up the true structure of $[(Zr_6-Co)Cl_{15}]$. (There are no bonds that link atoms between these interpenetrating nets and the local symmetry of the cluster remains unchanged when the calculation is performed in this way.) Thus, the space group for the calculation was $Pm\bar{3}m$ instead of $Im\bar{3}m$. Crystallographic coordinates were used in the calculation—no structural optimization was performed.[13] Kohn−Sham eigenvalues are shown in Figure 6; these were obtained using the JMW (Janak−Moruzzi−Williams) local spin-density exchange-correlation functional.[71] A calculation using the alternative VWN (Vosko−Wilk−Nusair) functional[72] gave virtually indistinguishable results (on the scale of Figure 6), except for a uniform upward level shift of approximately 0.08 eV. A double-numeric basis set was used and a frozen innercore approximation was employed (frozen 1s2s on Cl, frozen 1s2s2p on Co, frozen 1s2s2p3s3p3d on Zr). Experimentation on this and related cluster systems using nonlocal functionals is underway.

Supporting Information Available: Spectra of all NMR data (11 pages). See any current masthead page for ordering and Internet access instructions.

JA9713789

(71) Janak, J. F.; Moruzzi, V. L.; Williams, A. R. *Phys. Rev. B* **1975**, *12*, 1257−1261.

(72) Vosko, E. B.; Wilk, L.; Nusair, M. *Can. J. Phys.* **1980**, *58*, 1200−1211.